Journal of Materials Chemistry A

Accepted Manuscript

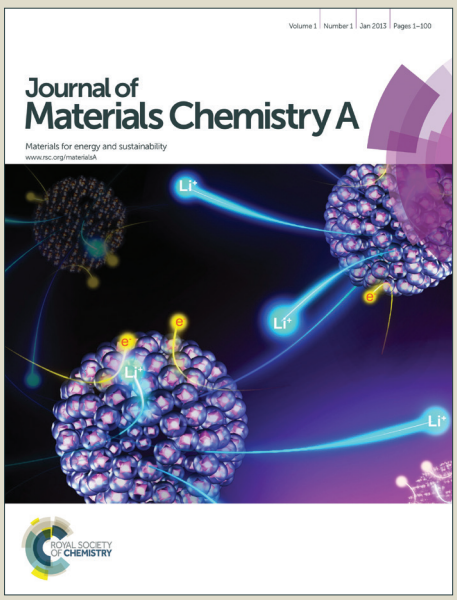

ROYAL SOCIETY OF CHEMISTRY

www.rsc.org/materialsA

Journal Name

RSCPublishing

ARTICLE

Study on Advanced $Ce_{0.9}La_{0.1}O_2/Gd_2Zr_2O_7$ Buffer Layers Architecture Towards All Chemical Solution Processed Coated Conductors

Cite this: DOI: 10.1039/x0xx00000x

Received 00th January 2012,
Accepted 00th January 2012

DOI: 10.1039/x0xx00000x

www.rsc.org/

Y. Zhao,[a] L. Ma,[a,b] W. Wu,[a,c] H.-L Suo,[b] and J. C. Grivel[a]

Chemical solution deposition is a versatile technique to deposit functional oxide films with low cost. In this study, this approach was employed in view of growth of multi-layered second generation high temperature superconductors ("coated conductors") with high superconducting properties. Both the $Ce_{0.9}La_{0.1}O_2/Gd_2Zr_2O_7$ buffer layer stack and the 200 nm thick $YBa_2Cu_3O_7$ (YBCO) superconducting layer were sequentially deposited on textured NiW substrates by using metal-organic deposition routes. The surface texture of the $Gd_2Zr_2O_7$ barrier layer deteriorates when the film thickness increases up to 80 nm, although the global texture retains a sharp biaxial orientation as determined by conventional X-ray diffraction. We paid particular attention on improvements of the surface quality in terms of crystallographic orientation and local flatness after depositing a $Ce_{0.9}La_{0.1}O_2$ thin film as cap layer. From comprehensive analysis of the surface morphology and misorientation maps reconstructed by electron backscattering diffraction technique, it is found that these improvements are mainly attributed to i) the preferential nucleation of $Ce_{0.9}La_{0.1}O_2$ crystals on the $Gd_2Zr_2O_7$ grains with desirable orientation, ii) the predominant two-dimensional growth of the $Ce_{0.9}La_{0.1}O_2$ crystals in the layer. Moreover, the microstructure and superconducting performance of the YBCO superconducting layer were thoroughly characterized and compared with those of films deposited on single crystal substrates using the same technique. A promising critical current density of 2.2 MA/cm^2 (77 K, self-field) was achieved on such an all-chemical derived configuration, demonstrating the high quality of the buffer layer stack and the feasibility of using all chemical-solution routes for the fabrication of low-cost coated conductors.

Introduction

The main text of the article should go here with headings as appropriate. The rapid development of the second generation high temperature superconductors (2G HTS, YBCO based coated conductors) in terms of superconducting performance and industrialization level holds the promise for a revolution in emerging energy applications. The main challenges for material science focus on further improvements of the performance of the coated conductors through low-cost routes. To realize the epitaxial multi-layer architecture in 2G HTS tapes, either physical or chemical film deposition techniques have been investigated and employed in the fabrication processes worldwide. So far, physical deposition approaches adopted by most groups/companies have yielded superior superconducting performance,[1, 2, 3] because of well-established knowledge and rigorous growth conditions (such as high-vacuum and limited growth rate). On the other hand, chemical solution deposition (CSD) processes which enable operation under normal or low-vacuum conditions have received less attention.[4] From an economic point of view, however, chemical deposition route could reach lower price targets considering both lower capital investments and relatively high growth rates of the films. In order to be competitive versus physical deposition approaches, more and more efforts have recently started to focus on further understanding of fundamental issues for CSD routes, including coating techniques,[5] solution chemistry,[6,7] film nucleation and growth.[8,9] Comprehensive knowledge however is still far away from being achieved.

In the all-CSD routes for coated conductor manufacture, biaxial orientation of the oxide films (both buffer layers and superconducting layers) transfer from highly textured Ni based tapes. Additionally, the cap layer (defined as the buffer layer close to the superconducting layer) plays an essential role on the nucleation of the YBCO layer, and consequently has a strong influence on its superconducting performance.

Compared to the microstructural characteristics (lattice mismatch, roughness and texture), several key surface properties including termination, polarity and catalytic activity remain poorly explored for cap layers.[10] The best candidates for a cap layer deposited by chemical routes so far are cerium oxide based materials, which possess a high melting temperature (~2500 ^{o}C) and stable cubic *fcc* (fluorite) structure.[11] Up to date, cerium films with various dopants have been investigated in view of further enhancing/multi-functionalizing the cap layer performance. Recently, we proposed and developed La doped CeO_2 ($Ce_{0.9}La_{0.1}O_2$, CLO) as a cap layer for an all-chemical derived coated conductors' configuration.[12] An YBCO layer grown on a CLO buffered yttrium stabilized ZrO_2 (YSZ) template exhibited high performance (>3 MA/cm^2), which is comparable with that of films grown on single crystalline $LaAlO_3$ by a low-fluorine metallic organic deposition route.[13] Comparing with pure CeO_2, the main advantages of the CLO as cap layer are: almost perfect lattice-match with YBCO and superior surface properties resulting from the high grain boundary mobility due to the La^{3+} dopant. It is believed that both would be beneficial for the nucleation and growth of YBCO layers.

In this work, as a further step toward enhancing the understanding of the key factors for developing all-chemical solution coated conductors. CLO is employed as cap layer on a $Gd_2Zr_2O_7$ (GZO)/NiW technical template, where GZO serves as barrier layer against the diffusion between the YBCO film and the metallic substrate. The surface properties of the CLO cap layer with respect to the GZO/NiW templates are thoughtfully characterized by means of electron backscattering diffraction (EBSD) and scanning electron microscopy (SEM) techniques. The improvement of the surface quality after depositing the CLO cap layer is discussed based on a self-epitaxy mechanism. Eventually, a full coated conductor structure with an YBCO/CLO/GZO/NiW constitution was achieved via an all-chemical solution deposition route to assess the compatibility of the films in a complete multi-layer structure.

Experimental

Synthetic procedures

The textured Ni5W alloy substrates used in this study were purchased from Evico GmbH. Prior to coating, the substrates were annealed in 5%H_2/N_2 flowing gas at 850 ^{o}C for 20 min followed by ultrasonic ethanol cleaning for 5 min and compressed air drying. GZO layers were deposited by using a propionates-based metal-organic solution with a fixed total cation concentration of 0.4 mol L^{-1}. The dip coating technique was used for preparing the films under ambient conditions. After immersing the substrate into the precursor, withdrawal speeds in the range of 20- 40 mm/min were applied. The coated films were dried in air for several minutes and directly inserted into an alumina-tube furnace for crystallization, as reported previously.[14, 15]Additionally, a multiple coating procedure was also used in order to increase the film thickness, i.e., the coating and annealing processes were repeated two or three times.

The precursor solution used for coating the CLO layer was synthesized by dissolving the reagents Cerium (III) and Lanthanum (III) 2,4-pentadionates (both from Aldrich) in stoichiometric amount in propionic acid at 150 ^{o}C until the color of the solution changed from light yellow to dark brown. The total cation concentration of the precursor was fixed at 0.2 mol L^{-1}. The substrate cleaning, solution coating and annealing were applied for obtaining CLO cap layers were similar to the GZO layer. The annealing atmosphere for both GZO and CLO layers was 5%H_2/N_2 forming gas.

To assess the quality of the CLO/GZO/NiW buffer layer stack, a 200 nm thick YBCO layer was deposited by the low-fluorine (LF-) metal-organic deposition route.[13] In this LF- solution, only the stoichiometric amounts of yttrium and barium sources are reacted with TFA, while a fluorine free copper salt is synthesized by dissolving copper acetate in an excess amount of acrylic acid. After mixing and rotary evaporation, the total cation concentration was adjusted to 1.5 M by adding a certain amount of methanol. The precursor was spin-coated on a 5 mm× 5 mm buffered substrate. The heat treatment procedure, including pyrolysis, crystallization and oxygenation were performed as reported previously on the single crystal substrates. For comparison, the YBCO films were also deposited on CLO/YSZ and $LaAlO_3$ single crystal substrates under the similar conditions.

Structural and superconductivity characterization

The phase and texture of the films were investigated by a four-circle diffractometer (Bruker D8) using Cu Kα radiation. EBSD measurements were carried out in a SEM (Zeiss Supra 35) equipped with a detector from HKL Technology. Surface texture of the CLO and GZO layers without any post-treatment were characterized by EBSD in an area about 430 × 390 μm^2 under normal operating conditions (electron energy of 15 kV in high-current mode). The Kikuchi patterns were automatically analyzed by the data handling software package (Channel 5). To evaluate the surface texture quality, the indexing rate on sample surface is extracted from the EBSD mapping without any *noise reduction* operation. The surface morphology of the films was evaluated by the same SEM with an in-lens detector. A DualScope atomic force microscope(AFM, DME Danish Micro Engineering A/S, Denmark) with a silicon tip is also used to evaluate the surface roughness. The superconducting transition temperature (T_c) was determined by resistance-temperature measurements in a Quantum Design Physical Property Measurement System (PPMS®) using the four-point method. The critical current densities, J_c, were calculated based on the Bean model using the opening of the hysteresis loops measured by a vibrating sample magnetometer (VSM, CRYOGENIC cryogen free measuring system) under a magnetic field applied perpendicular to the plane of the films.

Results and discussion

Thickness dependence of texture quality in the $Gd_2Zr_2O_7$/NiW template

In order to guarantee a sufficient barrier function of the buffer layer used in coated conductors, barrier layers with a certain thickness are definitely needed. Additionally, the microstructure of the barrier also plays an essential role against metal elements diffusion from the substrate. Defects, such as cracks, voids and grain boundaries can act as shortcuts for element diffusion at high temperatures.[16] Although the precursors, films thicknesses and annealing procedures are key points to determine the texture quality of the CSD-buffer layers, there is seemingly no significant difference in terms of microstructure of rare-earth zirconates layers especially for the thick films prepared by mono-coating routes. Similar sponge-like microstructures with a high density of nanovoids are commonly observed by several groups in the films body as well

as on the surface of CSD buffer layers,[14, 17-20] despite the materials, solution synthesis routes and the heat treatment processes varying. Up to date, no direct evidence is found to explain the formation of such structural features. It is, nevertheless, believed that porosity is related to the gas releasing during the early stage of heat treatment when metal organic precursors start decomposing into crystalline or amorphous oxides. In previous works, we obtained a nanovoid-free structure in a 20 nm thick, highly textured GZO film, indicating a strong correlation between the microstructure and the thickness of the film prepared by a mono-coating process.[21] In this study, in view of obtaining a similar microstructure (i.e., void-free or low porosity) in thick GZO barrier layers, a multi-coating route is employed rather than increasing the thickness in a mono-coated film. First, the thickness dependence of the texture quality in the GZO/NiW template was quantitatively investigated by means of X-ray diffraction and EBSD techniques, as plotted in Fig. 1. We noticed the similar trends of c-axis orientation extracted from XRD theta-2theta scans and the in-plane texture quality determined by (222) GZO phi-scans with increasing the film thickness, indicating a sharp texture on all the GZO films up to 80 nm thickness. Apparently, a little drop of c-axis orientation percentage in the 80 nm thick GZO film results from the presence of the GZO (222) reflection with low intensity. This undesirable GZO (222) reflection was also discerned by an XRD area-detector in our previous study, where two texture components (i.e., sharp <220> (004) texture and random orientation) coexist in the films.

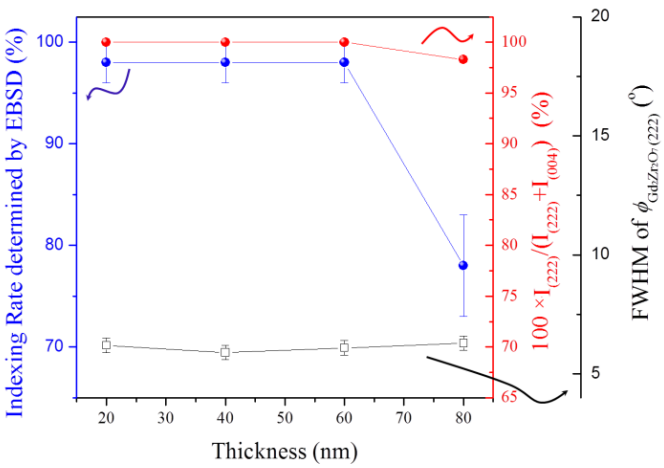

Figure 1 Thickness dependence of $Gd_2Zr_2O_7$ layers of the global and surface texture determined by conventional XRD and EBSD technique

Overall, the difference in global texture between the 80 nm thick and the other thinner GZO films is minor. However, thickness has a significant importance for surface crystallization as illustrated in the EBSD maps collected on the sample surface, as shown in Fig. 2 for two representative films with 60 nm and 80 nm thickness. Both misorientation maps exhibit similar granular structures, being indicative of texture transferring from the underlying NiW substrates. The indexing rate of the 60 nm thick GZO film is as high as 98.5%, with most of area within the individual NiW grains being well indexed (i.e., most of the un-indexed points are located along the grain boundaries of the NiW substrate beneath and on some large surface contaminations pointed by short arrows in the figures). In contrast, the 80 nm thick GZO film only yields an indexing rate of 78% in this selected area, while the GZO (222) pole figure shown as inset still demonstrates the highly biaxial texture for these indexed regions.

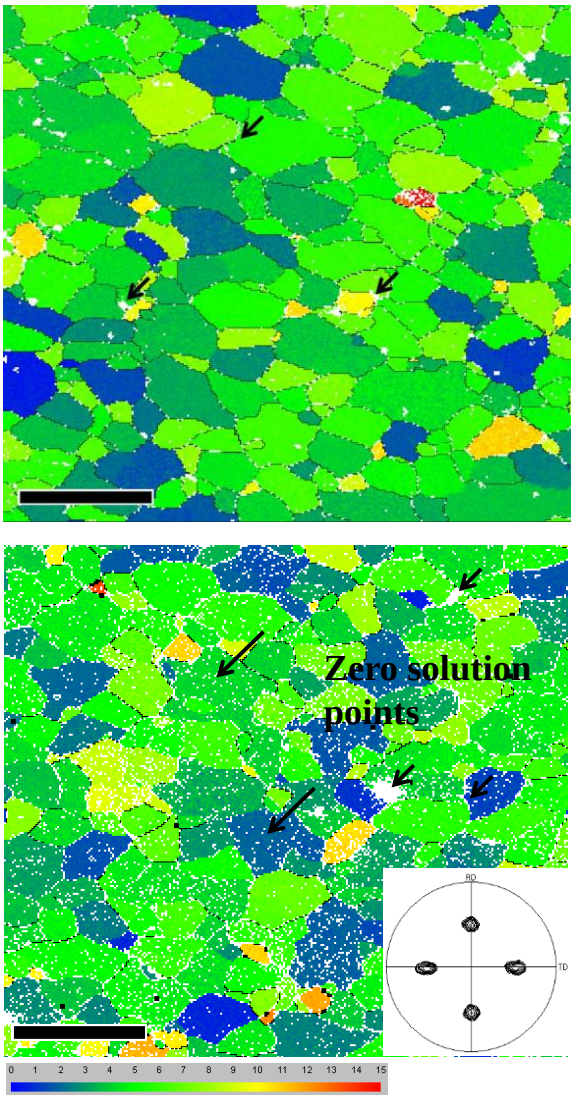

Figure 2 Misorientation maps acquired from the 60 nm and 80 nm thick $Gd_2Zr_2O_7$ layers (upper and lower), where the inset is the $Gd_2Zr_2O_7$ (222) XRD pole figure calculated from this region. Highlighted colours (from blue to red in the colour bar) represent tolerance angles deviating from the ideal orientation in degree, while zero solution points are represent in white, shown as arrows (short arrows for grain boundaries, particles and twin grains inherited from the substrate, and long arrows for the unsolved points within an individual NiW grains). The scale bars for both maps are 100 μm. Note that for comparison, *Noise-reduction was not performed*.

All the layers discussed in this paper exhibit similar roughness, i.e. r.m.s. values in the range from 2 nm to 5 nm on each individual NiW grain, which are comparable with that of NiW substrates. Therefore, the surface roughness has little influence on the quality of the Kikuchi patterns in this case. And a closer examination of this second map reveals that a large amount of

the un-indexed points are randomly distributed within the individual underlying NiW grains. Given that the grain size of the NiW substrate is larger than that of the GZO films by several order, nano-sized GZO particles on an individual NiW grain are expected to nucleate and grow exactly in the same conditions. The influence of the substrate texture and morphology is therefore very limited. The main reason for those un-indexed points is the poor texture quality locally on the sample surface. According to Monte Carlo simulations[22, 23], the lateral resolution of the EBSD technique is in the order of 50 nm to 100 nm depending on the operating conditions (current, voltage, etc). Thus each Kikuchi pattern obtained on the present GZO films includes information integrated in an area consisting of several GZO grains. As a consequence, only when the entire region (several GZO nano-grains involved) illuminated by an electron beam exhibits a single texture component, will a clear Kikuchi pattern appear, and subsequently being indexed by the program. Actually, it is not surprising to find a relatively poor texture on the surface of thicker films. When the film thickness is increased through applying a multi-coating route, there is a probability of introducing defects at the interface. The inhomogeneous release of residual carbon, which is the essential issue for obtaining highly epitaxial films grown by chemical solution methods, can also be involved.

Growth of a $Ce_{0.9}La_{0.1}O_2$ cap layer on top of a thick GZO barrier layer

A 20 nm thick CLO cap layer was deposited on an 80 nm thick GZO layer in order to investigate the improvement of the surface quality. The surface morphology before and after CLO cap layer deposition was observed by SEM, as shown in Fig. 3. The 80 nm thick GZO layer is rather dense as expected, and consists of equiaxed grains with dome-top. The lateral grain size (G.S.) is in the range from 10 nm to 40 nm. The image contrast in the local region also reveals the height differences in the sample surface, i.e., dark regions are relatively deeper than the bright ones (more visible in the inset of the Fig.3). On the contrary, the CLO layer exhibits a quite different surface morphology in terms of flatness, geometry of the grains, and lateral G.S. (around 100 nm). It can be seen that the whole surface is covered by square-shaped grains with atomical flat-top, except for a small portion of nano-sized pores at grain boundaries.

Combining with the crystallographic orientation analysis, it can be also deduced that the top of the CLO crystal is CLO (002), which is parallel to the normal direction of the NiW substrate (NiW (002)), while the edges of the CLO crystals are CLO <220> i.e., parallel to the transverse/ rolling direction of the NiW substrate (NiW<001>). The coherence between the crystallographic orientation and the geometrical alignment are indicative of a high biaxial texture quality in the CLO deposited on the top of GZO/NiW template. Moreover, the local flatness of the buffer layer stack is significant improved, as evidenced by the portion of the dark region that is reduced from 26% to 8% after the CLO layer deposition.

Additionally, the surface texture of the CLO layer is also confirmed by EBSD technique shown in Fig. 4. The indexing rate in this layer reaches 98.5%, which is 20% higher than that of the GZO layer. The uniform colors within the area defined by the underlying individual NiW grains suggest that those un-indexed regions were perfectly covered by CLO crystals with sharp texture.

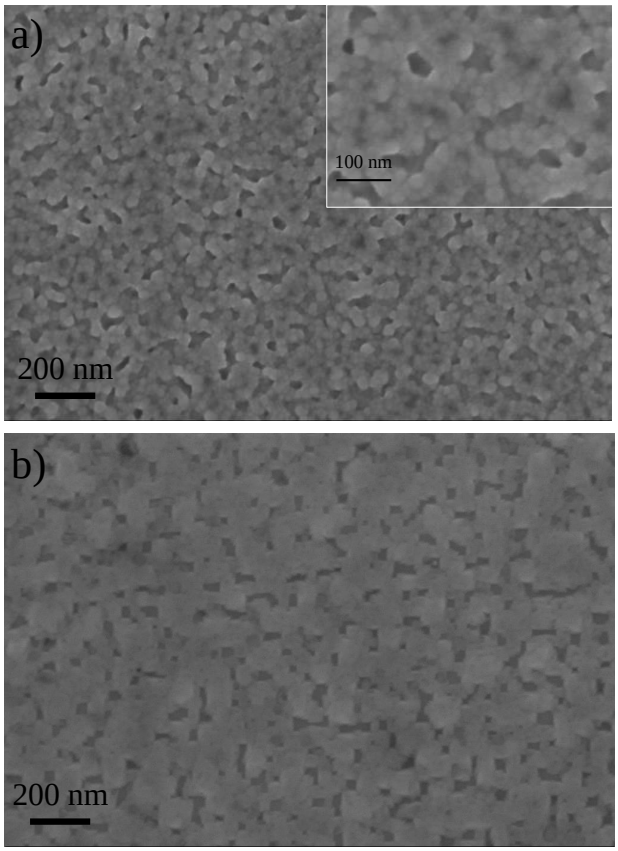

Figure 3 SEM images of the 80 nm thick $Gd_2Zr_2O_7$ layer before a) and after b) depositing the $Ce_{0.9}La_{0.1}O_2$ cap layer.

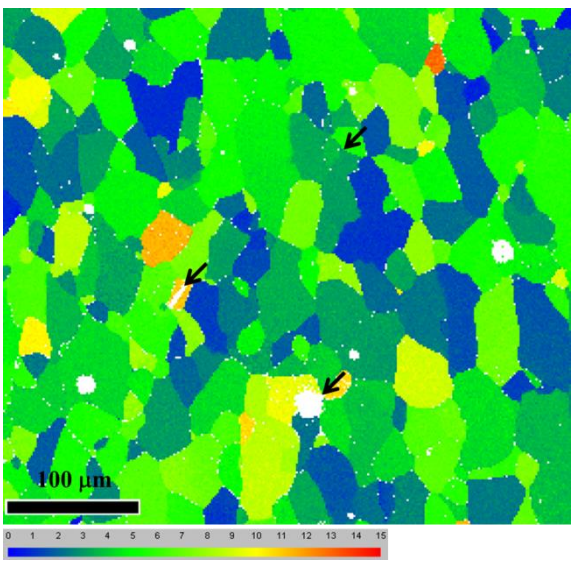

Figure 4 Misorientation map acquired from the $Ce_{0.9}La_{0.1}O_2$ cap layer grown on an 80 nm thick $Gd_2Zr_2O_7$ layer.

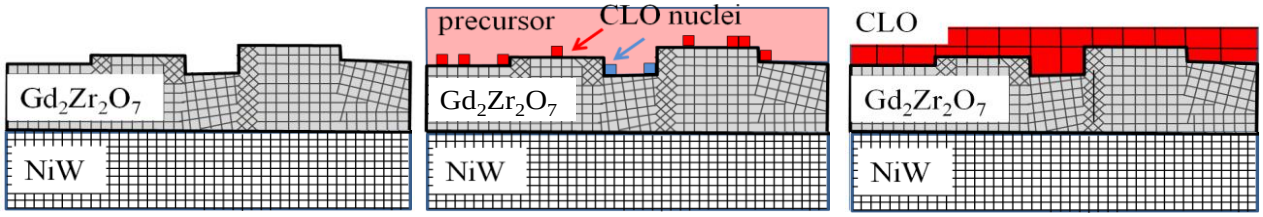

Figure 5 Schematic of the nucleation and growth processes of the $Ce_{0.9}La_{0.1}O_2$ cap layer on the $Gd_2Zr_2O_7$ layer. For simplification, the both the GZO and the CLO layers grown on an individual NiW grain are taken into consideration. The grids with different tilted angles represent the crystallographic orientations of the NiW substrate, the GZO layer and the CLO layer. The red squares represent the CLO nuclei with favored epitaxial orientation, while the blue ones being with less epitaxial orientations or random orientations.

To shed light on this surface improvement behavior, both nucleation and growth characteristics are taken into consideration. First, it was found that the grains with good texture quality generally have larger crystallite size, consequently with less strain, which would be energetically favorable for the nucleation of the layer on the top.[24] Texture improvements were observed in several multilayer stacks, such as CeO_2 on IBAD-GZO substrates,[25] YBCO on LMO/epi-MgO/IBAD-MgO substrates.[26] Similar mechanism probably also drive the nucleation of the CLO grown on the GZO layer, i.e. a CLO crystals preferably nucleate at those GZO grains with sharp texture due to minimized interface energy. Secondly, an atomically-flat surface in CeO_2 based thin films on either single crystal or metallic substrates was observed, which is strongly govern with several certain critical conditions, e.g., thickness and annealing temperature.[27, 28] It is also worth noting that another prominent feature associated with this morphology in both cases is the two-dimensional growth mode, as demonstrated by a much larger lateral grain size with respect of the thickness. This is one of the most essential prerequisites for improving the poor surface texture and smoothness of the thick GZO layer in this study. Based on the classical grain-growth models of polycrystalline films, a grain with a favored orientation has growth advantages, i.e., growing at the expenses of grains with less-favored orientation. Taking the advantage of the preferential nucleation and growth, the biaxial orientated CLO nuclei are with higher density, and are subsequently able to further develop mainly within the plane, thus covering the GZO regions even with poor biaxial texture.

A schematic summary of the growth process of the CLO cap layer responsible for the surface improvement is proposed and shown in Fig. 5. In the GZO/NiW templates, the surface quality in terms of the texture and the flatness is locally not optimum. After depositing a CLO layer, the nuclei have the preferential orientation nucleation, i.e., nucleation favorably occurs at interfaces with GZO <220> (004) orientation, while the nucleation density would be much lower on surface with other orientations. Consequently, a larger amount of CLO nuclei with desirable texture component CLO <110> (002) are able to further develop and cover most of the film surface by consuming the amorphous precursor or the smaller crystals forming on the top of the poorly textured GZO grains, taking the advantage of the two-dimensional growth mode.

Structural and superconducting properties of the YBCO layers

First, the XRD θ-2θ scan, YBCO (103) pole figure, (005) rocking curve and (103) phi scan were routinely performed in

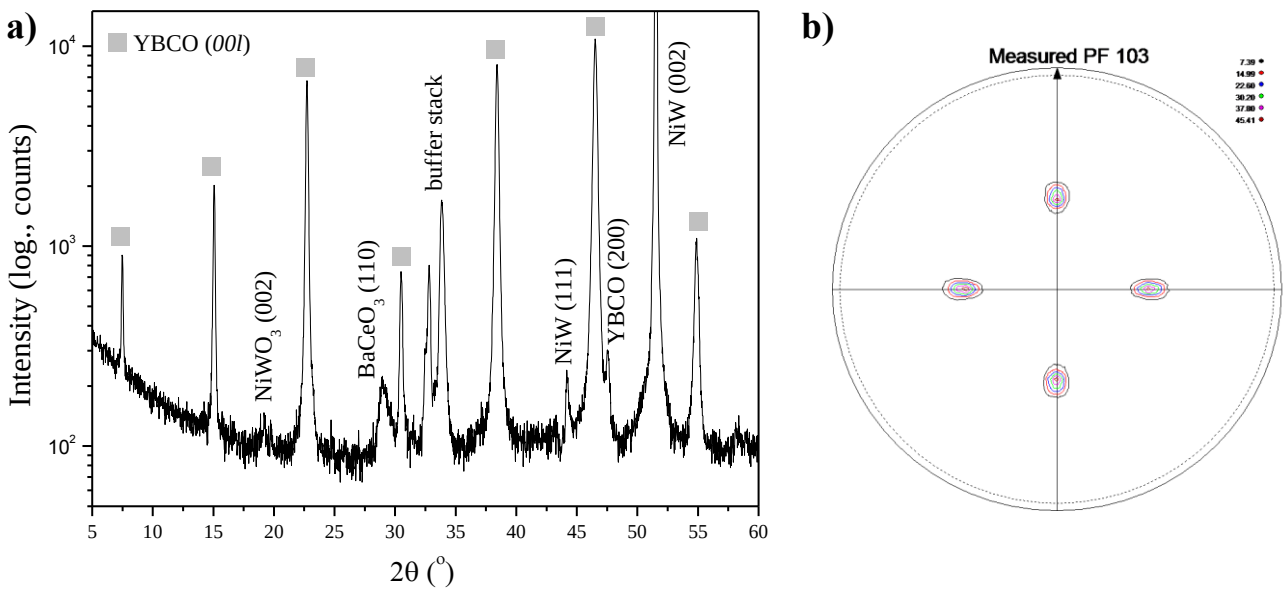

Figure 6 Conventional XRD analysis of a fully structured YBCO/ $Ce_{0.9}La_{0.1}O_2$ / $Gd_2Zr_2O_7$/NiW stack a) θ-2θ scan, b) YBCO (103) pole-figure.

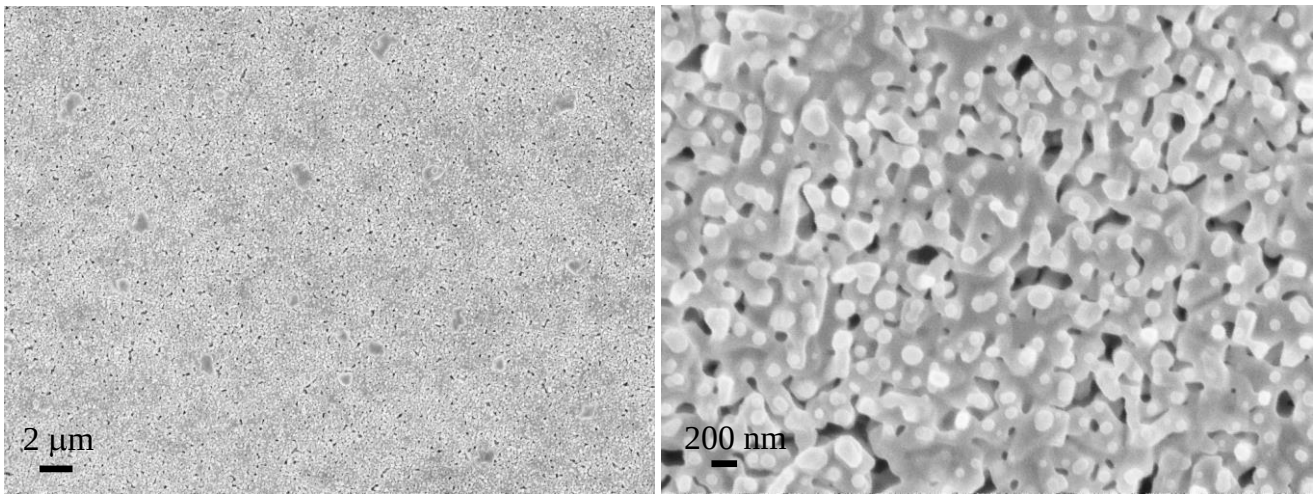

Figure 7 SEM images of the surface of a fully structured YBCO/$Ce_{0.9}La_{0.1}O_2$ /$Gd_2Zr_2O_7$/NiW.

order to obtain global structure information of the YBCO layer deposited on the all-chemical buffered NiW substrate. As show in Fig.6 a), strong YBCO (00l) peaks with minor secondary diffractions can be seen, being indicative of a sharp c-axis orientation. The presence of some impurities, $BaCeO_3$ (almost randomly orientated) and$NiWO_4$ (partly textured) also evidence the inevitable interactions between the YBCO and the buffered substrate even at low growth temperature (740 °C). Only four-fold concentrated poles in the YBCO (103) XRD pole-figure (Fig. 6 b) confirm the high quality of the in-plane and out-of plane texture. The FWHM value of the YBCO (005) rocking curve and the YBCO (103) phi-scan are 5.1°, and 7.5° (average), respectively, which are comparable with corresponding values for the buffer layers. These results imply that the formation of these secondary phases most likely happens after the YBCO nucleation. The YBCO nuclei with high degree of biaxial texture are seemingly able to develop further by consuming the intermediate phases, while the YBCO formed at the interface simultaneously reacts with the cap layer during the dwell stage. The morphology of the film observed by SEM is shown in Fig. 7. Generally, the film is homogeneous, smooth and almost featureless. No distinguishable grain boundary from the underlying NiW substrate is visible, demonstrating the planarization of the metallic substrate after depositing the buffer layer stack. From the high magnification SEM picture, it is clearly seen that the plate-like YBCO grains are larger than 200 nm in diameter. Besides this, it can be noticed that the microstructure is inhomogeneous at sub-micrometric scale, i.e., dense and porous regions coexist. A similar feature was also observed in MOD-YBCO films deposited on either a buffered single crystal (CLO/YSZ) or a $LaAlO_3$ single crystal in a similar temperature range.[13] It is therefore believed that such a structure is probably connected with the coarsening behavior resulting from the limited atomic mobility at relatively low growth temperature.

The temperature dependence of the normalized resistance (R-T plot) was obtained by the four-points contact technique on the YBCO layer deposited on the all-chemical buffered substrate, as shown in Fig. 8 a). The superconducting transition occurs between 86 K and 90 K, with a transition width ΔTc of about 2.7 K as shown in the inset of Fig 8a). The high resistance ratio of R (285 K)/(100 K)≥2.5 and linear resistance that extrapolates

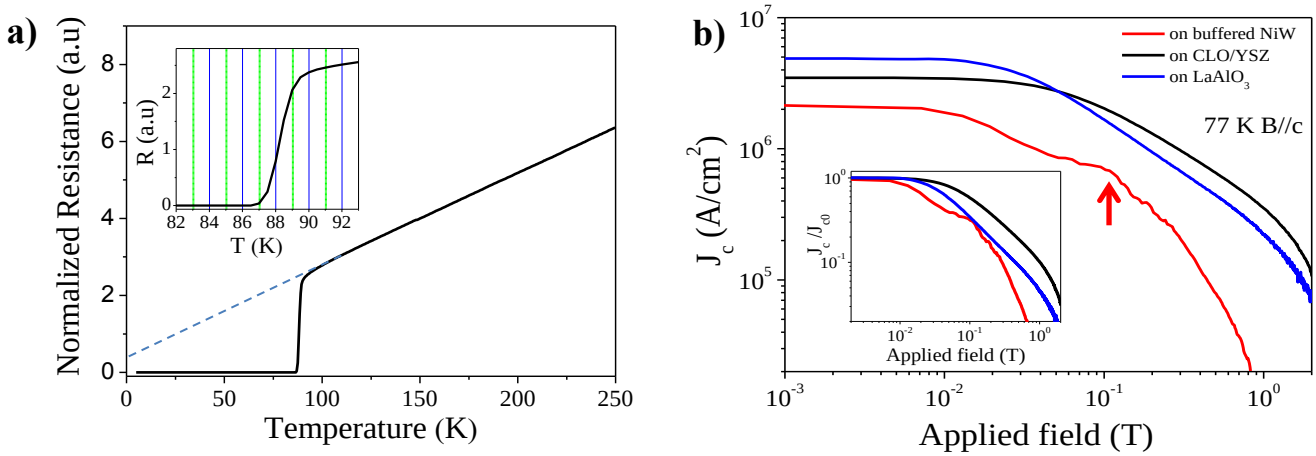

Figure 8 a) Four-probe transport measurement of the temperature dependence of the normalized resistance, where the dash line show the extrapolation of the linear temperature part of the resistance line to low temperatures, and the inset is the magnification of the transition. b) Double logarithmic plots of J_c vs. magnetic field B measured at 77 K for the YBCO/$Ce_{0.9}La_{0.1}O_2$ /$Gd_2Zr_2O_7$/NiW stack and the reference samples (grown on the CLO/YSZ single crystal at 740 °C and grown on $LaAlO_3$ single crystal at 800 °C). Inset: J_c versus magnetic field normalized with J_c at self-field.

to zero almost at 0 K in the R-T plot are typical features of high quality YBCO films with little grain boundary scattering in the normal state.[29] The $J_c(B)$ at 77 K of the YBCO film was calculated from the hysteresis loops measured by VSM, and is shown in Fig. 8 b). For comparison, the $J_c(B)$ *of* YBCO films grown on a buffered single crystal (CLO/YSZ) and on a $LaAlO_3$ single crystal are also plotted in Fig. 8 b). In the double-log scale, similar $J_c(B)$ behaviors were observed for all three YBCO films, *i.e.*, three regions including a plateau at low fields (up to the accommodation field, B^*), a power-law dependence $J_c(B)$ and high-field limit where J_c decreases rapidly. We noticed a small hump (pointed by an arrow) at around 200 mT for the YBCO film grown on the technical substrate, which is absent in the curves for YBCO grown on the two single crystals. This anomaly could be associated with a grain boundary effect or with a second type of field-activated pinning centers attributed to oxygen defects.[30, 31] It is worth pointing out that a J_c value of the YBCO film grown by the all-chemical route reaches 2.2 MA/cm^2, which is promising compared with those of the films grown on similar substrates by vacuum physical deposition techniques.[12, 32] The relatively lower J_c values of the YBCO film on the technical substrate than on the single crystals are due to grain-boundary limitations. Finally, the normalized $J_c(B)$ dependence at 77 K were plotted and shown in the inset of Fig. 8 b). A smaller B^* and sharper drop-off of $J_c(B)$ at higher external fields ($>B^*$) for the film grown on the technical substrate is also discerned, which is most likely due to the presence of low angle grain boundaries in the YBCO films inherited from the NiW substrate underneath.[33]

Conclusions

In this paper, we investigated the role of CLO films as cap layer in the YBCO/CLO/GZO/NiW coated conductors configuration made by all chemical-solution routes. The thickness dependence of the GZO layers deposited by a multi-coating approach shows that the surface texture deteriorates when the film thickness increases up to 80 nm, although the global texture determined by conventional XRD exhibits sharp biaxial orientation comparable with those of thinner films. Most interestingly, a significant improvement of the surface quality in terms of flatness and crystallographic orientation is observed after depositing CLO films on top of the 80 nm thick GZO template. The square-shaped CLO crystals with flat-top fully cover the granular GZO grains with dome-like top. By checking the EBSD misorientation maps, the indexing rate of the Kikuchi patterns increases from 78% to 98.5% after CLO layer deposition, which is a clear indication of enhancement of the desirable texture on the surface.

Preferential orientation nucleation occurring on textured GZO regions and the predominant two-dimensional growth of the CLO layer are two main reasons for such improvement of the surface quality. Finally, an YBCO film was grown on the buffer layer stack by a low-fluorine metal-organic decomposition route. Compared with those films deposited on CLO buffered YSZ and blank $LaAlO_3$ single crystals, a promising J_c value of 2.2 MA/cm^2 was obtained on such all chemical-solution processed coated conductor structure. This study suggests the essential role of using this type of CLO films as a cap layer, and demonstrates the feasibility of a high quality coated conductors structure grown by low-cost chemical-solution routes.

Notes and references

[a] Department of Energy Conversion and Storage, Technical University of Denmark, Frederiksborgvej 399, DK-4000 Roskilde, Denmark.
[b] College of Materials Science and Engineering, Beijing University of Technology, 100124 Beijing, China.
[c] Department of Electrical Engineering, Shanghai JiaoTong University, 200240 Shanghai, China.

1 A. Usoskin, T. Bubelis, A. Rutt, et, al. "Long-length YBCO coated conductors manufactured in medium size pilot production line based on pulsed laser deposition", 2014, *ICEC/ICMC Conference*.
2 Y. Shiohara, T. Taneda and M. Yoshizumi, *Jpn. J. Appl. Phys.*, 2012, 51, 010007.
3 D. W. Hazelton and V. Selvamanickam, *Proceedings of the IEEE*, 2009, 97, 1831-1836.
4 M. Bäcker. "Recent Progress in Development of All-Solution Coated Conductors at Deutsche Nanoschicht", 2013, *Applied superconductivity conference.*
5 M. Vilardell, X. Granados, S. Ricart, et.al., *Thin Solid Films*, 2013, **548**, 489-497.
6 G. Pollefeyt, S. Clerick, P. Vermeir, et.al. , *Inorg. Chem.*, 2014, **53**, 4913-4921.
7 M. Erbe, J. Hanisch, T. Freudenberg, et.al., *J. Mater. Chem. A*, 2014, **2**, 4932-4944.
8 X. Obradors, T. Puig, M. Gibert, et.al., *Chem. Soc. Rev.*, 2014, **43**, 2200-2225.
9 T. M. McCleskey, P. Shi, E. Bauer, et.al., *Chem. Soc. Rev.*, 2014, **13**, 2141-2146.
10 V. F. Solovyov, T. Ozaki, A. Atrei, et. al., *Sci. Rep.*, 2014, **4**, 4627.
11 C. H. Steele, *Solid State Ionics*, 2000, **129**, 95-110.
12 Y. Zhao, X.-F. Li, A. Khoryushin, et.al., *Supercond. Sci. Technol.*, 2012, **25**, 015008.
13 Y. Zhao, W Wu, X Tang, et. al., *CrystEngComm*, 2014, **16**, 4369-4372.
14 Y. Zhao, J.-C. Grivel, A B Abrahamsen, et.al., *IEEE Trans. Appl. Supercond.*, 2011, **21**, 2912-1915.
15 Y. Zhao, J.-C. Grivel, M. Napari, D. Pavlopoulos, J. Bednarčík and M. von Zimmermann., *Thin Solid Films*, 2012, **520**, 1965-1972.
16 T. Aytug, M. Paranthaman, K.J. Leonard, et.al., *J. Mater. Res.*, 2005, **20**, 2988-2996.
17 L. Molina, H. Tan, E. Biermans, et.al., *Supercond. Sci. Technol.*, 2011, **14**, 065019.
18 R.B. Mos, T. Petrisor Jr., M.S. Gabor, et. al., *Thin Solid Films*, 2013, **513**, 491-498.
19 W. Zhao, A. Norman, S. Phok, et. al., *Physica C*, 2008, **468**, 1092-1096.
20 N. Vyshnavi, I. V. Driessche. *Prog. Solid State Ch.*, 2012, **40**, 57-77.
21 Y. Zhao, J.-C. Grivel, M. Liu, et. al. *CrystEngComm*, 2012, **14**, 3089-3095.
22 S. X. Ren, E. A. Kenik, K. B. Alexander, A. Goyal, *Microsc. Microanal.*, 1998, **4**, 15-22.
23 A. Goyal, S.X. Ren, E.D. Specht, et. al., *Micron*, 1999, **30**, 463-478.
24 T. Taneda, M. Yoshizumi, T. Takahashi, et. al., *IEEE Trans. Appl. Supercond.*, 2013, **23**, 6601005.
25 V. Matias, J. Hänisch, E. J. Rowley, and K. Güth, *J. Mater. Res.*, 2009, **24**, 125-129.

26 V. Matias, B. J. Gibbons, J. Hanisch, et, al., *IEEE Trans. Appl. Supercond.*, 2007, **17**, 3263-3265.
27 M. Coll, A. Pomar, T. Puig, et. al., *Appl. Phys. Express*, 2008, **1**, 121701.
28 Y Zhao, J.-C. Grivel. *CrystEngComm.*, 2013, **15**, 3816-3823.
29 P. Norton, A. Goyal, J.D. Budai, et, al., *Science*, 1996, **274**, 755-757.
30 H. Hojaji, S. Hu, A. Barkatt, D.D. Davis, A.N. Thorpe, *Physica C*, 1992, **195**, 135-144.
31 M. Daeumling, J.M. Seuntjens, D.C. Larbalestier, *Nature*, 1990, **346**, 332-335.
32 H. Huhtinen, M. Irjala, P. Paturi, et, al., *Physica C*, 2012, **472**, 66-74.
33 D.T. Verebelyi, D.K. Christen, R. Feenstra, *Appl. Phys. Lett.*, 2000, **76**, 1755-1757.

